International Journal of Heat and Mass Transfer 52 (2009) 79–91

Contents lists available at ScienceDirect

International Journal of Heat and Mass Transfer

journal homepage: www.elsevier.com/locate/ijhmt

Subcooled flow boiling and microbubble emission boiling phenomena in a partially heated microchannel

Guodong Wang, Ping Cheng *

Ministry of Education Key Laboratory of Power Machinery and Engineering, School of Mechanical and Power Engineering, Shanghai Jiaotong University, Shanghai 200240, PR China

ARTICLE INFO

Article history:
Received 3 March 2008
Received in revised form 14 June 2008
Available online 29 August 2008

Keywords:
Subcooled flow boiling
Microbubble emission boiling
Microchannel
Microheater

ABSTRACT

A simultaneous visualization and measurement study has been carried out to investigate subcooled flow boiling and microbubble emission boiling (MEB) phenomena of deionized water in a partially heated Pyrex glass microchannel, having a hydraulic diameter of 155 μm, which was integrated with a Platinum microheater. Effects of mass flux, inlet water subcooling and surface condition of the microheater on subcooled flow boiling in microchannels are investigated. It is found that MEB occurred at high inlet subcoolings and at high heat fluxes, where vapor bubbles collapsed into microbubbles after contacting with the surrounding highly subcooled liquid. In the fully-developed MEB regime where the entire microheater was covered by MEB, the mass flux, the inlet water subcooling and the heater surface condition have only small effects on the boiling curves. The occurrence of MEB in microchannel can remove a large amount of heat flux, as high as 14.41 MW/m^2 at a mass flux of 883.8 kg/m^2 s, with only a moderate rise in wall temperature. Therefore, MEB is a very promising method for cooling of microelectronic chips. Heat transfer in the fully-developed MEB in the microchannel is presented, which is compared with existing subcooled flow boiling heat transfer correlations for macrochannels.

1. Introduction

It is well known that subcooled boiling phenomena is characterized by boiling occurring adjacent to the heated surface while the surrounding fluid is at a subcooled condition. As early as in 1934, Nukiyama [1] had studied subcooled *pool* boiling of water about a heated wire at a superheated temperature, and reported the first boiling curve in terms of heat flux versus degree of wall superheat. For the past several decades, subcooled *flow* boiling in channels has also attracted considerable attention [2–7] because of its applications in nuclear reactor cores, lasers, as well as vehicle power electronics, where the high-heat-flux cooling is required. Kandlikar [2] divided subcooled flow boiling of water into partial boiling, fully-developed boiling, and significant void flow regions, and a comprehensive methodology with appropriate correlations was presented to predict the heat transfer in each region. Prodanovic et al. [3] investigated subcooled flow boiling of water on a vertical annular test section (12.7, 22, and 780 mm in inner diameter, outer diameter, and length, respectively) at bulk liquid velocities from 0.08 to 0.8 m/s, and subcooling from 10 to 30 K. They found three different bubble behavior regions: low-heat-flux region, isolated bubble region, and significant bubble coalescence region. A semi-empirical correlation for determining the variation of bubble size and lifetime was proposed. Subcooled flow boiling heat transfer and bubble characteristics of R-134a were investigated in a number of papers [4–6]. However, the effects of mass flux and liquid subcooling on the onset of nucleate boiling (ONB) reported in these papers were not consistent.

In 1986, Inada et al. [8] studied *pool* boiling about a heated copper cylindrical tip submerged in water at the subcooling of 30 K with the void probe method. They discovered the existence of microbubble emission boiling (MEB) phenomena where coalesced bubbles generated on the heated surface at high heat flux were broken to many microbubbles after contacting with the surrounding liquid at a high degree of subcooling. It was found that the heating surface was not easily dried out and noisy sounds were heard when MEB occurred. Subsequently, Shoji and Yoshihara [9] measured the critical heat flux (CHF) of highly subcooled pool boiling of water on a thin heated wire and found that the CHF could reach 10 MW/m^2. With the aid of a high-speed camera and a microscope, they found that MEB occurred on the wire at the subcooling of more than 40 K. Wang et al. [10] carried out similar experiments with the aid of a high-speed camera and a microscope on pool boiling of water about a horizontal thin heating platinum wire in subcooled alcohol or water. They observed that nucleation jet flows from the wire were formed and some jets evolved to miniature bubbles. It appears that the physical mechanism for the

* Corresponding author.
E-mail address: pingcheng@sjtu.edu.cn (P. Cheng).

0017-9310/$ - see front matter © 2008 Elsevier Ltd. All rights reserved.
doi:10.1016/j.ijheatmasstransfer.2008.06.031

Nomenclature

A_h	area of microheater (m^2)
C_p	specific heat of liquid ($J\,kg^{-1}\,K^{-1}$)
D	hydraulic diameter of channel (m)
E	forced convection heat transfer enhancement factor (–)
G	mass flux ($kg\,m^{-2}\,s^{-1}$)
h_{fg}	latent heat of evaporation ($J\,kg^{-1}$)
h	heat transfer coefficient ($W\,m^{-2}\,K^{-1}$)
I	electric current (A)
k	thermal conductivity of silicon substrate ($W\,m^{-1}\,K^{-1}$)
M	molecular weight (–)
Nu	Nusselt number (–)
p	pressure (bar)
Pr	Prandtl number (–)
q	heat flux ($MW\,m^{-2}$)
R	resistance (Ω)
Re	Reynolds number (–)
S	suppression factor (–)
t	time (s)
T_f	bulk liquid temperature $T_f = (T_{out} + T_{in})/2$ (°C)
T_{in}	inlet water temperature (°C)
T_{out}	outlet water temperature (°C)
T_h	microheater temperature (°C)
T_{sat}	saturation temperature (°C)
ΔT_b	change in bulk temperature, $\Delta T_b = T_h - T_f$ (°C)
ΔT_{sat}	superheat $\Delta T_{sat} = T_h - T_{sat}$ (°C)
ΔT_{sub}	subcooling $\Delta T_{sub} = T_{sat} - T_b$ (°C)
V	electric voltage (v)

Greek symbols

ρ	density ($kg\,m^{-3}$)
σ	surface tension ($N\,m^{-1}$)
μ	dynamic viscosity ($N\,s\,m^{-1}$)

Subscripts

eff	effective heat flux
expt	experimental
h	microheater
in	inlet
loss	heat loss
l	liquid
nb	nucleate boiling
out	outlet
pred	predicted
r	precise resistor
sp	single-phase
tp	two-phase
v	vapor

occurrence of miniature bubbles observed by Wang et al. [10] was similar to the occurrence of microbubbles in the MEB [8,9]. With the aid of a high-speed camera and a microscope, Suzuki et al. [11–13] carried out the first series of experiments on microbubble emission boiling in subcooled *flow boiling* in rectangular and circular minichannels with a localized heat source at a velocity ranging from 0.25 to 2.5 m/s and inlet water subcooling from 20 to 40 °C. The rectangular channels were 1–17 mm in height and 12–24 mm in width with a heat source of 10–20 mm in width and 10–50 mm in length, and the circular channels were 5, 10, and 16 mm in diameters with a heat source 10 mm in length on the wall. They found that the degree of subcooling was a key parameter for the occurrence of MEB. At low liquid subcooling of 20 K, MEB was unstable and it could easily turn into film boiling. At the liquid subcooling of 40 K and velocity of 0.5 m/s, the maximum heat flux could reach to 10 MW/m^2 without burnout, which greatly exceeded the present cooling limit for electronic equipment.

Tange et al. [14] presented a hypothesis of microbubble generation during MEB: Under high subcooling and high heat-flux conditions, intense vaporization at the bottom of a bubble adjacent to the heated surface, and rapid condensation at the bubble top may cause strong bubble interface oscillation, leading to microbubble emission in a highly subcooled liquid. According to this hypothesis, both high degree of subcooling and high heat flux are important factors for MEB generation. The reasons why MEB was not frequently observed in subcooled flow boiling experiments in the past [2–6] might be attributed to the following reasons: (i) the simultaneous conditions of high heat flux and high degree of subcooling were not satisfied in most of the flow boiling experiments which were usually carried out in a long tube heated uniformly with a heat flux less than 1 MW/m^2; (ii) if the imposed heat flux on the wall was high enough to initiate MEB in the upstream, the wall downstream would be burnout. Furthermore, since liquid subcooling was decreasing along the flow direction due to the uniform heating, there was insufficient subcooling to sustain MEB in the downstream even if no burnout occurred; and (iii) no high-speed camera and microscope were used to observe flow boiling in these large heated tubes in the past. It may be concluded that MEB can only be observed with the aid of a high-speed camera and a microscope for a channel with high inlet subcooling at high heat flux over small heated surfaces (such as in a line heat source) or partial heating.

Recently, a great deal of interest has been devoted to the study of boiling heat transfer in microchannels heated uniformly on the wall [15–17] with applications to cooling of microelectronic chips. In this paper, we have performed simultaneous visualization and measurement study to investigate subcooled flow boiling in a *partially heated* microchannel integrated with a platinum microheater, having a hydraulic diameter of 155 μm. With the aid of a high-speed camera and a microscope, microbubble emission boiling (MEB) was observed above the microheater in a microchannel at high heat flux and with a high degree of inlet water subcooling. Effects of mass flux, inlet water subcooling and surface condition of the microheater on MEB are investigated. In addition, typical MEB patterns in microchannels are captured with the aid of a microscope and a high-speed video recording system. Heat transfer in MEB in the microchannel is presented and compared with existing low boiling heat transfer correlations for mini/macrochannels.

2. Description of the experiment

2.1. Experimental setup

Fig. 1 shows the experimental apparatus and the flow circuit. It consisted of four major components: a working fluid loop, a test section integrated with a heating unit, a data acquisition system, and a visualization system. The deionized water, being pushed either by a high pressure tank (at high mass flux) or a syringe pump (at low mass flux), flowed successively through a degassing unit (to remove the dissolved gas), a constant temperature bath (to ensure a certain inlet subcooled water temperature), a 0.5-μm-filter (to remove solid particles), a needle valve (to regulate the mass flux pushed by the high-pressure tank) and finally the test section. After the test section, water was collected in a container at atmospheric pressure. When the high-pressure tank was used to drive

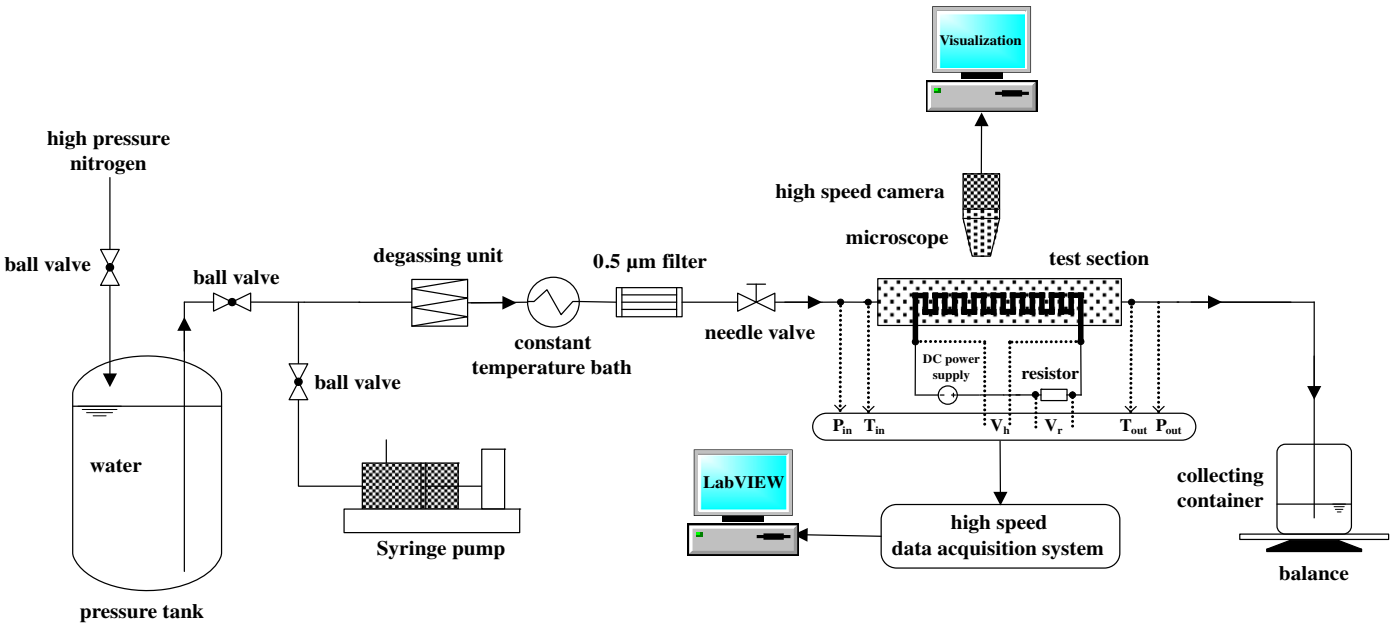

Fig. 1. Experimental test loop.

the working fluid, the average mass flux of water was determined by calculating mass increment per unit time in the container, which was placed above a precision electronic balance.

The heating unit was connected with a DC power supply and an electronic control circuit, in which the total voltage input supplied to the microheater, could be adjusted and controlled. A precise resistor ($R = 5\ \Omega$) was connected in series with the microheater and the voltage across the resistor, V_r, was measured. The current delivered to the microheater could be calculated from $I = V_r/R$, and the resistance R_h of the microheater could be calculated according to $R_h = V_h/I$, where V_h was the input voltage to the microheater. The average temperature of the microheater was determined from R_h, which will be discussed later in Section 2.3.

Two pressure transducers with a response time of 0.001 s were used to measure water pressures (P_{in} and P_{out}) at inlet and outlet of the microchannels. All pressure and voltage (V_r and V_h) signals were collected by a NI high-speed data acquisition system, and the LabView software was used to monitor the signals. A microscope with a maximum magnification of 20, and a high-speed camera (with a maximum frame rate of 5145 fps at full resolution of 512×512 pixels) were used to record flow patterns in the microchannel.

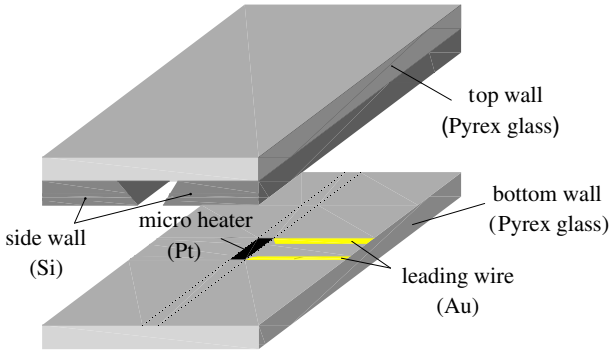

Fig. 2. Sketch of microchannel integrated with microheater.

2.2. Test section

As sketched in Fig. 2, the two side walls of the microchannel in the test section were etched in a ⟨100⟩ silicon substrate. The microchannel having a length of 15 mm was bonded from the top and bottom by two Pyrex glass plates. The top Pyrex glass plate allowed visualization of boiling phenomena in the microchannel. An integrated microheater was fabricated on the bottom Pyrex glass wall. The top width, bottom width, and depth of the trapezoidal microchannel were 427, 280, and 104 μm, respectively, and the microchannel had a hydraulic diameter of 155 μm.

The serpentine microheater, fabricated by using MEMS technique with a typical lift-off metallization application, is shown in Fig. 3a. It was located between 8.5 and 10.5 mm from the entrance at the bottom Pyrex glass wall of the microchannel as shown in Fig. 2. The microheater was made of a 500 Å. TiW film (for adhesion between Pyrex glass and platinum film) and 6000 Å platinum film were sputtered onto the bottom Pyrex glass plate coated with photoresist after a photolithography process. After lift-off in acetone, a similar photolithography process and 500 Å TiW film (for adhesion between platinum film and gold film) were repeated, and a gold pad with a thickness of 3000 Å acted as the leading wire. A very thin layer of silicon dioxide was deposited to protect the heater and form a smooth heating surface (approximately 50 nm in average roughness). The microheater, being 200 μm (width) × 2000 μm (length) in size, was much smaller than the bottom wall of microchannel having 280 μm in width and 15 mm in length. Fig. 3b shows detailed dimensions of a section of the microheater. The thin film platinum heater was 40 μm in width with each strip being 20 μm apart from its neighbors. The heater had an area of 0.28 mm^2, covering approximately 70% of the Pyrex glass plate.

2.3. Calibration of the microheater

Since platinum has a good linear relationship between resistance and temperature, the platinum microheater served not only as a heater but also a temperature sensor of the heated surface. By placing the microheater in a thermal bath, the relationship between the resistance and the averaged temperature of the

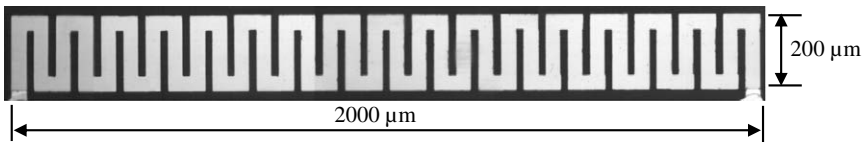

(a) the whole microheater

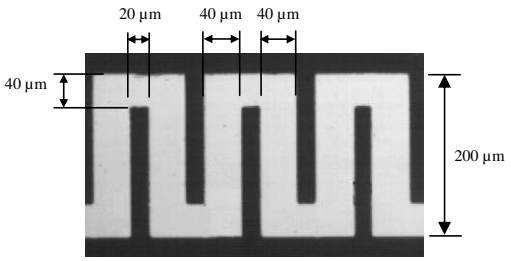

(b) part of the microheater

Fig. 3. Photos of the microheater.

microheater could be determined and calibrated. The resulted linear relationship between the temperature, T_h, and the resistance, R_h, of microheater is given by

$$R_h = 37.60082 \times (1 + 0.002588T_h) \quad (1)$$

2.4. Data reduction

Li et al. [18] conducted a detailed numerical simulation of forced convection heat transfer in silicon-based microchannel heat sinks with axial heat conduction in the wall taken into consideration. They found that approximately 40–60% of the heat flux (at $Re = 40$) was conducted from downstream part of the silicon-based heat sink into the upstream part of the heat sink due to axial heat conduction because of the high thermal conductivity of the silicon wafer. In the present experiment, a platinum thin film microheater sputtered on a Pyrex glass plate was used. Since the Pyrex glass had a low thermal conductivity, therefore, axial conduction in the microheater used in the present experiment was negligible compared to the heaters used by previous investigators [15–17] on their flow boiling experiments in microchannels.

We now discuss the determination of the effective heat flux (q_{eff}) absorbed by the water in the microchannel, and the conduction heat loss (q_{loss}) through the bottom Pyrex glass plate in this experiment. The total heat flux supplied to the microheater and the effective heat flux absorbed by the fluid were calculated according to:

$$q = V_h I / A_h \text{ and } q_{eff} = q - q_{loss} \quad (2a, b)$$

where $A_h = 0.28$ mm^2 is the area of the microheater. The conduction heat loss q_{loss} from the Pyrex plate was determined by the method used previously by Chen and Chung [19] as follows. Before the boiling experiment, the test section was turned upside down so that the heater faced downward in contact with the surrounding stagnant air. Under this condition, the heater was powered to reach wall temperatures as those in the boiling experiments. Twenty to thirty minutes were allowed for the heater to reach a steady state before measurements were taken. Thus, the conduction heat loss through the Pyrex glass plate was equal to the heat supplied by the microheater. This conduction heat loss was used to calculate the effective heat flux absorbed by the fluid from Eq. (2b) in the present flow boiling experiments. The average boiling heat transfer coefficient, h, of the microchannel is calculated from

$$h = q_{eff} / \Delta T_b \quad (3)$$

where ΔT_b is the average temperature difference between the microheater temperature T_h, and bulk temperature of water T_f, i.e., $\Delta T_b = T_h - T_f$ with $T_f = (T_{out} + T_{in})/2$ where T_{in} and T_{out} are inlet and outlet temperatures of water, respectively.

3. Results and discussion

3.1. Single-phase forced convection in a single microchannel

In order to assess whether the method for determination of the effective heat flux in this experiment was accurate, we first studied single-phase forced convection in the Pyrex glass microchannel prior to the onset of boiling. It is well known that the length required for the formation of a fully-developed laminar flow in a macrochannel can be estimated from $L_e/D_h = 0.057Re$. In the present experiment where the microchannel had a hydraulic diameter of 155 μm and using water ($Pr = 6.6$) as a working medium with $Re < 826.7$, the upstream length of 8.5 mm was more than sufficient to ensure that the flow was hydraulically fully-developed before reaching the microheater, while it was a thermally developing flow along the microheater.

A 3D single-phase heat transfer numerical simulation, with temperature dependent physical properties taken into consideration, was performed using the commercial software package "FLUENT" to investigate forced convection heat transfer characteristics in the microchannel before boiling occurred. Fig. 4 shows the 3D simulation results for the surface temperature distribution of the microheater for forced convection in the microchannel at $q = 3.31$ MW/m^2, $G = 294.6$ kg/m^2 s and $T_{in} = 20$ °C. It is shown that the water temperature increased along the flow direction from 360.0 K (i.e., 86.8 °C) at the beginning of the microheater to the highest temperature of 479.4 K (i.e., 206.2 °C) at the downstream side of the microheater. The average simulated surface temperature of the microheater was 417.8 K (i.e., 144.6 °C), which will be compared with experimental results prior to the onset of microbubble emission boiling in Section 3.2.

Fig. 5 shows a comparison of Nusselt numbers obtained from numerical simulation (with temperature-dependent physical properties) and experimental data for hydraulically fully-developed and thermally developing forced convection of water in the microchannel under three different heat fluxes at various Reynolds numbers up to $Re = 826.7$. The following conclusions can be drawn from this figure: (i) the good agreement between the numerical simulation and experimental data of Nusselt number confirmed that the method to deduce the effective heat flux, q_{eff}, was accurate; (ii)

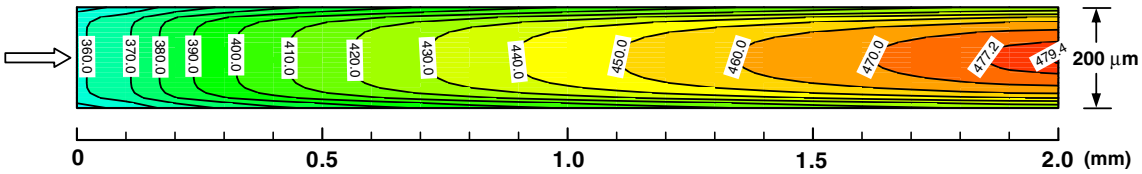

Fig. 4. Three-dimensional numerical results of temperature distribution on the microheater at q_{eff} = 3.31 MW/m^2, G = 294.6 kg/m^2 s, and T_{in} = 20 °C.

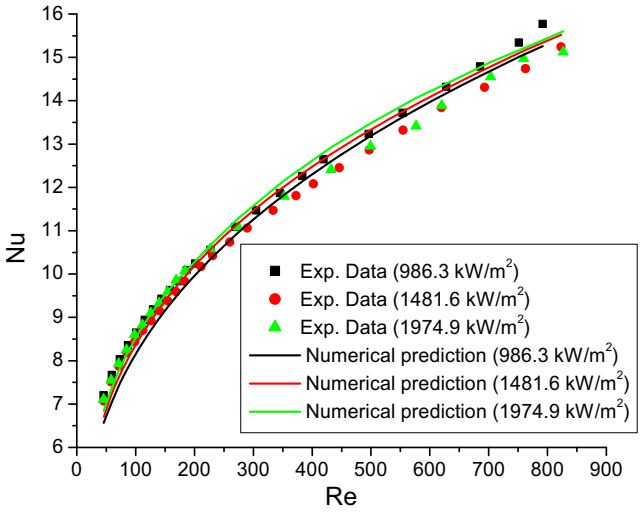

Fig. 5. Comparison of numerical predictions and experimental data for Nusselt number in microchannel at different heat flux.

the Nusselt number increased with increasing Reynolds number in the thermal developing flow as expected; and (iii) both the experimental data and numerical simulation show that heat flux has a small effect on the Nusselt number because fluid properties (thermal conductivity and viscosity) were varied with temperature, which was associated with heat flux.

3.2. Microbubble emission boiling phenomenon in subcooled flow boiling

Fig. 6a shows the subcooled boiling curve at constant mass flux condition of G = 294.6 kg/m^2 s and inlet water temperature at 20 °C, with heat flux increasing from 0 to 7.41 MW/m^2 (which caused the burnout of the microheater). It is shown that as the heat flux was gradually increased from 0 to 3.31 MW/m^2, the temperature of the microheater increased linearly to 140.3 °C. The linear variation of microheater surface temperature with respect to heat flux suggests that no boiling occurred, and the heat transfer was due to single-phase forced convective heat transfer as discussed in Section 3.1. Fig. 6b is an enlarged subcooled flow boiling curve on the transition region from single-phase flow to two-phase flow. Under the conditions of G = 294.6 kg/m^2 s and T_{in} = 20 °C, it is interesting to note that the single-phase forced convection region ended at a wall temperature of 140.3 °C (at a heat flux of 3.31 MW/m^2), which was well above the saturated temperature of T_{sat} = 100 °C (corresponding to the atmospheric pressure in the present experiment) because the Pyrex glass wall was very smooth and free of cavities. The measured average temperature of the microheater at 140.3 °C was comparable to the numerical simulated average temperature of 144.6 °C as mentioned earlier. In the following, the investigation on the onset of microbubble emission boiling (OMEB) at point 1 (Fig. 6b), developing MEB from points "1" to "4" and fully-developed MEB (after point "4") phenomena in a microchannel at G = 294.6 kg/m^2 s and T_{in} = 20 °C will be discussed. It is shown from Fig. 6a and b that a large amount of heat flux from 3.56 to 7.19 MW/m^2 was supplied with only a slight increase in wall temperature of the microheater from 137.1 to 146.7 °C during the fully-developed MEB regime before the occurrence of critical heat flux (CHF).

3.2.1. Onset of microbubble emission boiling

We now define the onset of microbubble emission boiling (OMEB) as the condition where a very small increase in the heat fluxes would cause the sudden appearance of MEB near the end of microheater where the maximum temperature occurred. For G = 294.6 kg/m^2 s, MEB began to appear at the downstream end of the microheater when the heat flux reached a value of 3.31 MW/m^2 and the average surface temperature of the microheater was 140.3 °C.

The OMEB can be attributed to the heterogeneous nucleation mechanism on a smooth surface free of cavities. According to Li and Cheng [20], the theoretical heterogeneous nucleation temperature, T_{nb}, for air-dissolved water is given by

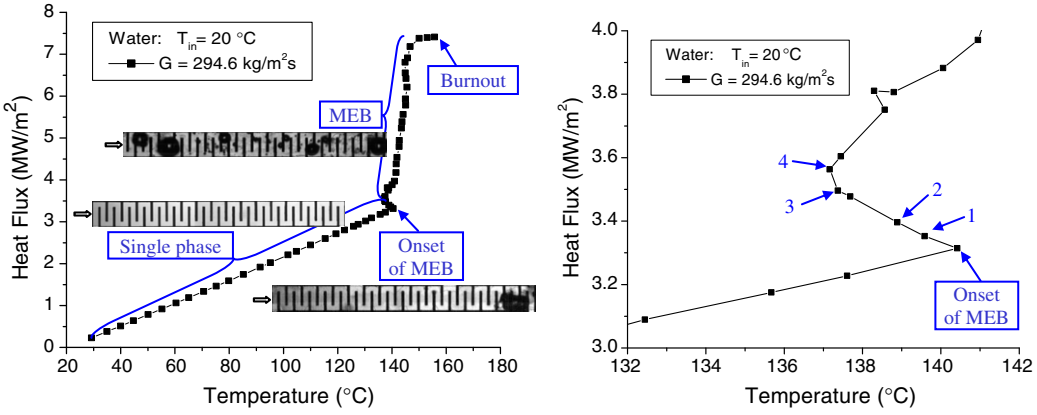

(a) boiling curve (b) Enlarged subcooled flow boiling curve

Fig. 6. Subcooled flow boiling curve of water at T_{in} = 20 °C and G = 294.6 kg/m^2 s.

$$T_{nb} - T_s = \frac{T_s \exp(C_g)}{h_{fg}\rho_v}\left(\sqrt{\frac{16\pi\sigma^3\omega}{3kT_{nl}\ln(N_0''kT_{nl}\psi/\mathrm{J\ h})}} - K_h C_g\right) \quad (4)$$

where C_g is the solubility of the dissolved gas, K_h the Henry's constant, ψ the surface available per unit bulk volume of liquid phase for heterogeneous nucleation, and ω the geometric correction factor for the minimum work required to form a critical nucleus. The heterogeneous nucleation temperature on a smooth surface with saturated dissolved air as calculated from Eq. (4) was approximately 504 K for water on a platinum surface with a contact angle of 20°. The reasons for the difference between the experimental value of 140.3 °C (i.e., 413.5 K) and the theoretical value of 504 K can be attributed to: (i) impurities in the water, (ii) submicron defects on the surface of the microheater, and (iii) some residual air in the water could decrease the incipience temperature as discussed in [20,21].

Fig. 7 is a sketch of the bubble behavior on the microheater during OMEB, which can be divided into three periods of time: bubble growth, bubble size fluctuation, and bubble collapse. After a bubble grew to a certain size, the bubble began to fluctuate in size due to non-equilibrium between the condensation at the bubble top and the evaporation from the vapor layer at the bubble base. Fig. 8a is a series of photos showing bubble behavior during bubble size fluctuation to bubble collapse. It can be seen from Fig. 8a (vi) that microbubbles (about 10 μm in diameter) were emitted during the bubble collapse due to condensation and instability of bubble interface. Fig. 8b shows that a bubble fluctuated in size between 40 and 120 μm in diameter before its collapse, thus confirming the earlier speculation by Tange et al. [14] about bubble fluctuations before collapsing. The corresponding surface temperature variation of the microheater is presented in Fig. 9, which shows that the instantaneous temperature of the microheater dropped from 140.3 to 133.5 °C during OMEB and increased again during the refilling of the superheated liquid. The instantaneous temperature drop during MEB in subcooled flow boiling is similar to that during the onset of nucleation in subcooled flow boiling [4,5]. In addition, it can be seen from Fig. 9 that the time from bubble growth to collapse was less than 10 ms during OMEB.

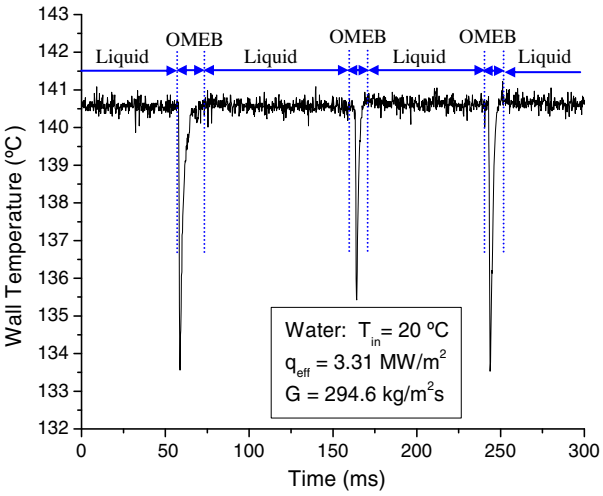

Fig. 9. Measurement of wall temperature at OMEB.

3.2.2. Developing microbubble emission boiling

With further increase in heat flux beyond the OMEB at constant mass flux of $G = 294.6\ \mathrm{kg/m^2\ s}$, the surface temperature suddenly decreased at point "1" and continued to decrease to the minimum temperature at point "4" as shown in Fig. 6b. We will refer to the regime from point "1" to point "4" where the wall temperature decreased as heat flux increased as the "developing MEB regime". The corresponding photos showing the developing MEB are presented in Fig. 10, where it is shown that MEB first occurred at end of the microheater at $q = 3.35\ \mathrm{MW/m^2}$ (a), moved upstream to the mid section when the heat flux is increased to $q = 3.40\ \mathrm{MW/m^2}$ (b), approached upstream section when $q = 3.50\ \mathrm{MW/m^2}$ (c), and fi-

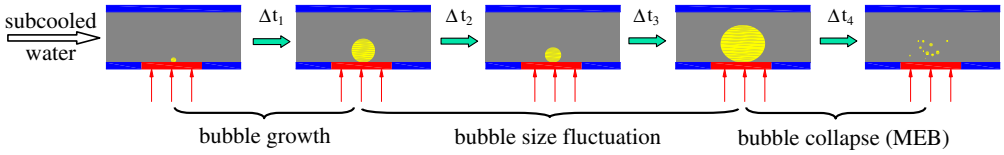

Fig. 7. Sketch of the bubble behavior in OMEB.

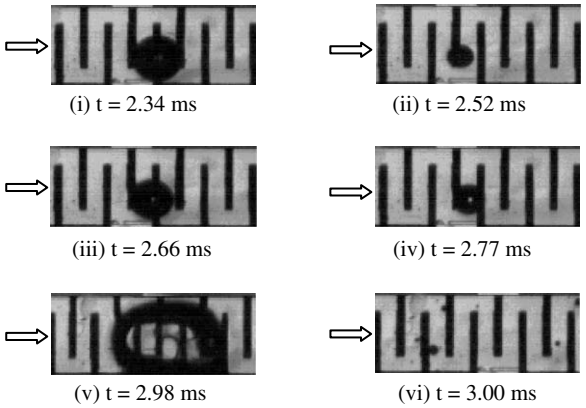

(a) Photos of bubble diameter fluctuation and collapse into microbubbles (taken at 44000 frame/s)

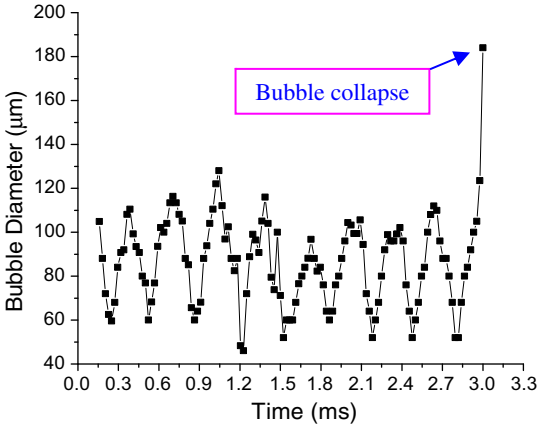

(b) Bubble size fluctuation with time

Fig. 8. Photos and sketch of bubble behavior in OMEB at $q_{eff} = 3.31\ \mathrm{MW/m^2}$, $G = 294.6\ \mathrm{kg/m^2\ s}$, and $T_{in} = 20\ °\mathrm{C}$.

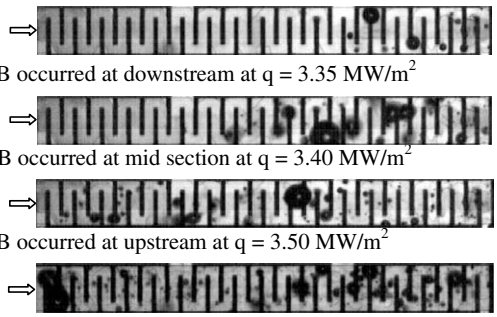

Fig. 10. Photos of developing MEB in the microchannel at $G = 294.6\ kg/m^2\ s$, and $T_{in} = 20\ °C$.

nally MEB occurred over the entire microheater at $q = 3.56\ MW/m^2$corresponding to point "4" where the temperature of the microheater was minimum. The temperature decrease from point "1" to point "4" was caused by the increasingly larger area in which MEB occurred from the end to the front of the microheater.

3.2.3. Fully-developed MEB and local dryout

The fully-developed MEB began when MEB occurred over the entire microheater and its surface temperature increased again as the heat flux was increased. Fig. 11a are a series of photos at $q = 6.21\ MW/m^2$ (with $G = 294.6\ kg/m^2\ s$ and $T_{in} = 20\ °C$) where bubbles formed over the entire microheater, and began to coalesce with each other and then collapsed and broke into microbubbles. This behavior was different from those during OMEB where bubbles fluctuated in size (see Fig. 8a) before collapsing. It can be seen from Fig. 11a that three bubbles formed into a large bubble over the microheater as a result of coalesce from (i) to (iii) in 0.0682 ms and collapse at 0.136 ms (vi). Due to condensation and instability of bubble interface between vapor and subcooled water, many micobubbles were emitted during the collapse of the bubble (iv–vi), and thus fully-developed MEB occurred on the microheater. Also, these microbubbles could serve as bubble embryo and promoted the MEB further. Fig. 11a shows that the period of MEB was about 0.14 ms which is rather short compared to that of a nucleated bubble in nucleate boiling which lasts longer than 1 ms [22]. The bubble behavior in fully-developed MEB to bubble collapse is sketched in Fig. 11b.

Bang et al. [5] pointed out that the CHF was the result of the dryout of the near-wall bubble layer consisting of small bubbles and interleaved liquid between the microheater and large vapor clots. A simultaneously visualization and temperature acquisition in Fig. 12 shows that vapor clots indeed occasionally occurred at downstream end of the heater when the heat flux was increased to $q_{eff} = 7.37\ MW/m^2$ (at $G = 294.6\ kg/m^2\ s$ and $T_{in} = 20\ °C$), and at which time the corresponding wall temperature increased instantaneously to as high as 270 °C due to the dryout of the near-wall bubble layer. However, due to the wetting and rewetting process, the dry spot was partially or completely condensed by subcooled liquid flow and did not cause burnout of the microheater. This sharp temperature rise occurred in about 0.1 s during the dryout of local microheater, and then dropped to normal temperature ranging from 130 to 150 °C as a result of MEB. Note that drastic temperature rises in Fig. 12b were a signal of the imminent burnout of the microheater.

3.3. Effects of mass flux, inlet water subcooling and surface condition of the microheater on MEB

To investigate the effects of mass flux and inlet water temperature on subcooled flow boiling in the microchannel, experiments were carried out at mass fluxes of $G = 294.6$, 589.2, and 883.8 $kg/m^2\ s$ with $T_{in} = 20$, 60, and 80 °C (i.e. $\Delta T_{sub} = 80$, 40, and 20 °C, respectively) by gradually increasing the heat flux. The ranges of inlet water temperature, mass flux, imposed heat flux, and corresponding microheater temperatures in these subcooled boiling experimental runs are listed in Table 1. For all of these cases, it can be seen that MEB in microchannel could remove a large amount of heat with only a moderate rise in wall temperature. Therefore, this heat transfer mode is very promising for next generation of chip cooling technology for microelectronic devices.

3.3.1. Effects of different mass fluxes on MEB

Fig. 13 shows effects of the mass fluxes ($G = 294.6$, 589.2, and 883.8 $kg/m^2\ s$) on boiling curves (in terms of heat flux versus temperature) with $T_{in} = 20\ °C$. It is shown that (i) at this high degree of subcooling of 80 °C, MEB occurred at all mass fluxes at sufficiently high heat flux, (ii) a higher heat flux was needed to initiated OMEB at higher mass flux, (iii) the superheat of the microheater in OMEB was larger at a higher mass flux; (iv) the mass flux had little effects on the boiling curves in the fully-developed MEB regime; and (v) the maximum heat flux without burnout increased as the mass flux was increased. For example, the heat flux was leveling off at 7.3 MW/m^2 when $G = 294.6\ kg/m^2\ s$ while the heat flux was as high as 14.41 MW/m^2 without reaching critical heat flux when the mass flux was increased to $G = 883.8\ kg/m^2\ s$. Fig. 13b is a comparsion of bubble sizes at different mass fluxes showing that the average bubble sizes were smaller as the mass flux was increased.

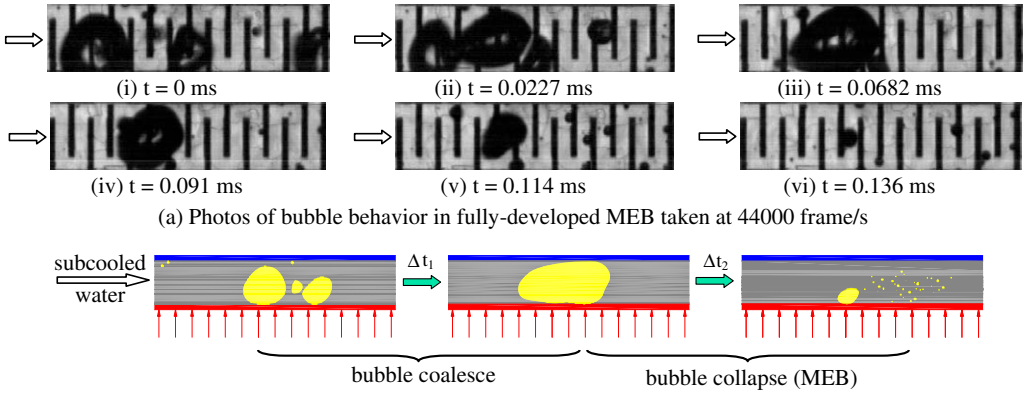

Fig. 11. Photos and sketch of bubble behavior in fully-developed MEB at $q_{eff} = 6.21\ MW/m^2$, $G = 294.6\ kg/m^2\ s$, and $T_{in} = 20\ °C$.

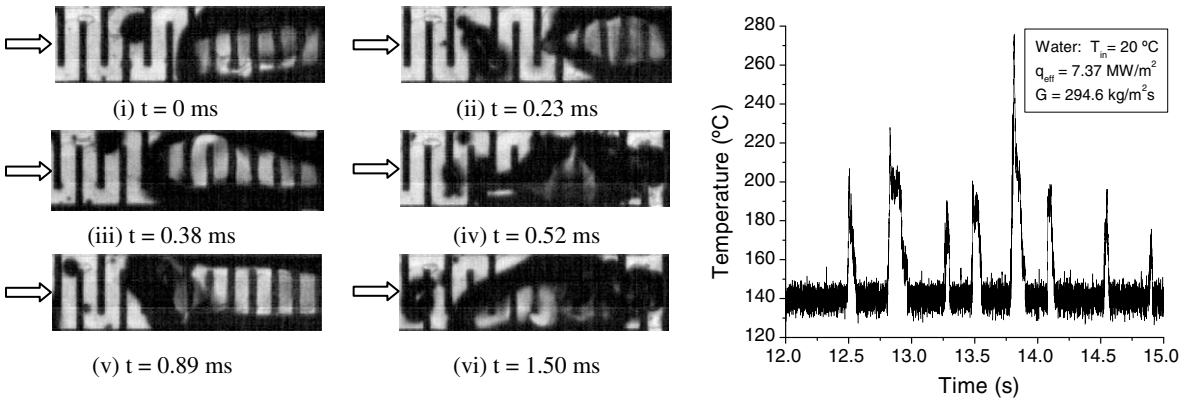

(a) Photos of vapor clots at downstream end of the microheater taken at 44000 frame/s

(b) Measurement of the microheater temperature fluctuation

Fig. 12. Photos of local microheater dryout and temperature fluctuation of the microheater at q_{eff} = 7.37 MW/m^2, G = 294.6 kg/m^2 s, and T_{in} = 20 °C.

Table 1
Microheater temperature and heat flux in microchannel in MEB at T_{in} = 20 and 60 °C

Inlet water temperature (°C)	Mass flux (kg/m^2 s)	Imposed heat flux		Corresponding heater temperature	
		From (MW/m^2)	To (MW/m^2)	From (°C)	To (°C)
20	294.6	3.56	7.19	137.1	146.7
20	589.2	5.31	12.44	139.6	159.1
20	883.8	6.48	14.41	145.4	165.9
60	589.2	3.40	7.14	147.2	155.3

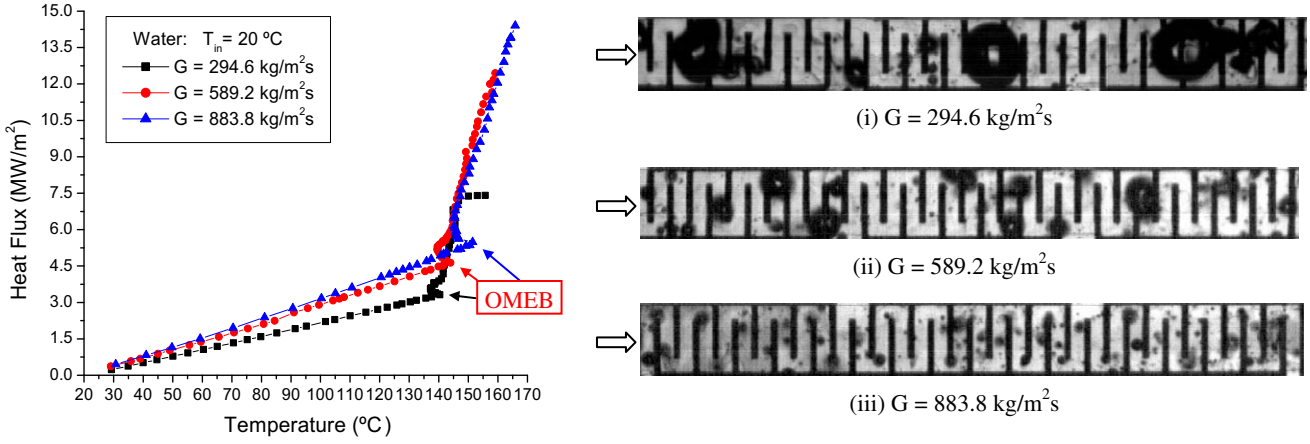

(a) Subcooled flow boiling curves

(b) Photos of bubble sizes at q_{eff} = 6.78 MW/m^2

Fig. 13. Effects of mass flux on subcooled flow boiling with T_{in} = 20 °C.

3.3.2. Effects of different inlet water subcoolings on MEB

Fig. 14 shows the effect of the inlet water temperature of 20, 60, and 80 °C, (corresponding to inlet water subcooling ΔT_{sub} of 80, 40, and 20 °C, respectively). on the subcooled flow boiling and MEB at mass flux of 589.2 kg/m^2 s. It is shown that (i) a higher heat flux and a lower temperature were needed to initiate the onset of microbubble emission for a higher degree of inlet water subcooling; (ii) in the fully-developed MEB, the boiling curves were not affected to a significant degree by inlet water subcooling; and (iii) the maximum heat flux increased as the degree of subcooling increased. For example, at a mass flux of 589.2 kg/m^2 s, the maximum heat flux was 5.08 MW/m^2 at ΔT_{sub} = 20 °C and it increased to 7.14 MW/m^2 at ΔT_{sub} = 40 °C; and (iv) although MEB occurred for the cases of high degree of subcooling of ΔT_{sub} = 80 and 40 °C, it did not occur for low degree of subcooling at ΔT_{sub} = 20 °C as will be discussed below.

Fig. 15a shows a series of photos on flow patterns at low degree of subcooling ΔT_{sub} = 20 °C for G = 589.2 kg/m^2 s and q_{eff} = 2.90 MW/m^2. It can be seen that at such low degree of inlet subcooling, the bubble continued to grow and elongate without collapsing and breaking into microbubbles, and therefore no MEB occurred. The corresponding flow patterns of elongated bubbles in the microchannels are sketched in Fig. 15b. When the heat flux was increased to q_{eff} = 4.07 MW/m^2, bubbles began to expand upstream and downstream as shown in Fig. 16a. An isolated bubble first nucleated in the upstream of the microchannel at t = 0 ms, and it grew up in size as it was flushed downstream from t = 0.70 ms to t = 0.95 ms. After it touched the channel walls, it began to expand in both upstream and downstream directions, as shown from t = 0.95 ms to t = 2.50 ms. When the inlet pressure was increased sufficiently to overcome the vapor bubble advancing

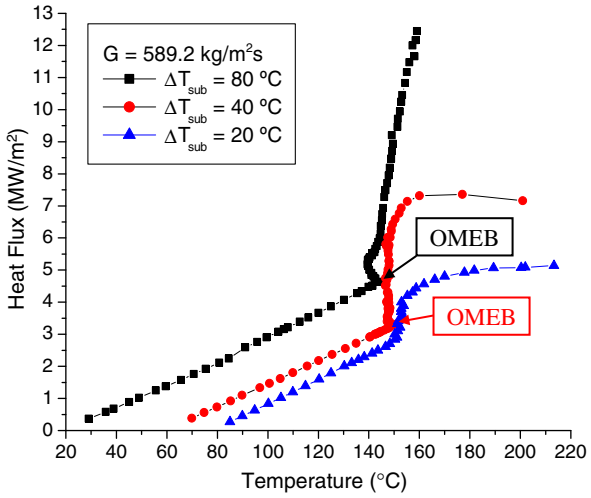

Fig. 14. Effects of inlet water subcooling on subcooled flow boiling curves with $G = 589.2$ kg/m^2 s.

upstream, incoming subcooled water rushed into the microchannels from t = 2.50 ms to t = 3.20 ms, thus beginning a new cycle. Under this condition, any small increase in heat flux from $q_{eff} = 4.07$ MW/m^2 would cause a large increase in wall temperature because of the upstream expansion of the vapor bubble (see the triangular dots in Fig. 14).

Fig. 16a is a series of photos on flow boiling with a low degree of subcooling of 20 °C at $q_{eff} = 4.07$ MW/m^2, and Fig. 16b is a sketch of the bubble expansion process where bubble expanded upstream and swept by the incoming subcooled water. As a result, the microheater temperature fluctuated periodically as shown in Fig. 17. It can be seen that the ranges of temperature fluctuation were from 180 to 255 °C. The maximum temperature corresponded to the condition where expanded long bubble covered the whole microheater where local dryout occurred instantaneously. The wall temperature dropped when subcooled water entered periodically. This temperature fluctuations were similar to those discussed previously in Refs. [15–17].

3.3.3. Effects of surface condition of the microheater on MEB

During the collapse of the coalesced bubble, surrounding cold water would suddenly rush into the empty space occupied by the bubble before its collapse, and hit the heater surface which was similar to a kind of cavitations, causing the erosion of the heater surface. Thus, after several runs of subcooled boiling experiments, it was found that OMEB did not occur and ONB occurred at many eroded sites instead.

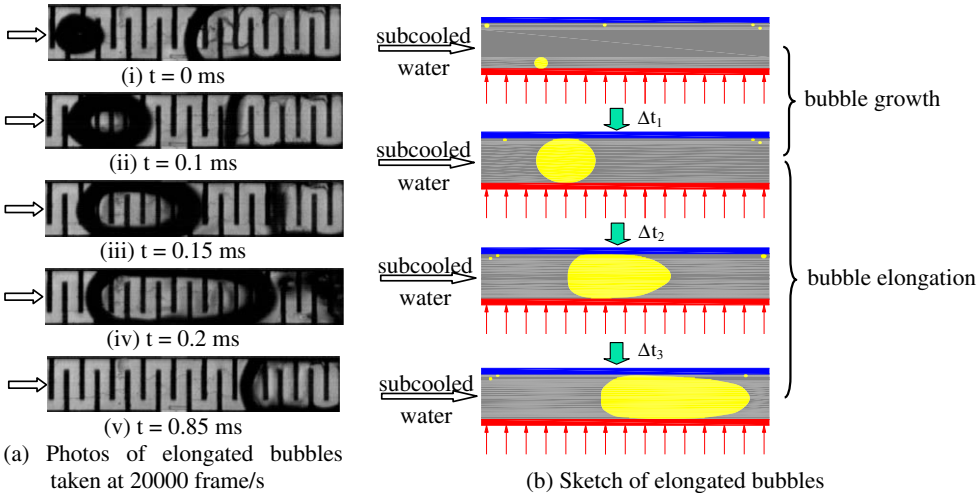

(a) Photos of elongated bubbles taken at 20000 frame/s

(b) Sketch of elongated bubbles

Fig. 15. Photos and sketch of elongated bubbles at $q_{eff} = 2.90$ MW/m^2, $G = 589.2$ kg/m^2 s, and $T_{in} = 80$ °C.

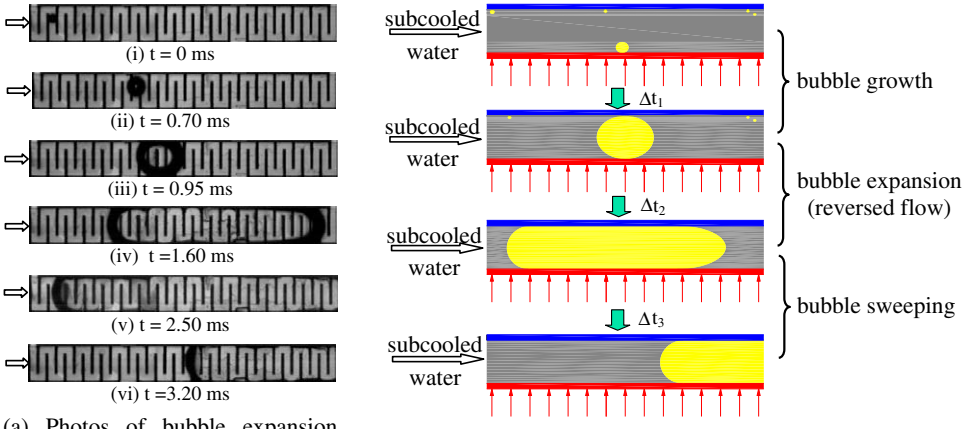

(a) Photos of bubble expansion taken at 44000 frame/s

(b) Sketch of bubble expansion

Fig. 16. Photos and sketch of bubble expansion toward both upstream and down downstream at $q_{eff} = 4.07$ MW/m^2, $G = 589.2$ kg/m^2 s, and $T_{in} = 80$ °C.

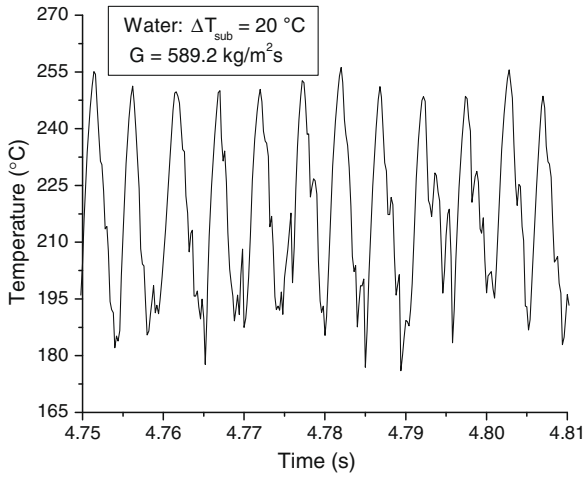

Fig. 17. Measurement of periodical temperature fluctuation of the microheater at q_{eff} = 4.07 MW/m^2, G = 589.2 kg/m^2 s, and T_{in} = 80 °C.

Fig. 18 compares the subcooled flow boiling curves of water for two types of surface conditions at G = 294.6 kg/m^2 s with T_{in} = 20 °C. The square dots were the experimental data when the microheater had a highly smooth surface. As mentioned earlier, it was observed that the wall temperature was extremely high at OMEB because of the lack of nucleate sites on the highly smooth Pyrex glass surface. The circular dots were the last experiment when the microheater had been eroded with many nucleated sites. The shape of the circular dots boiling curve in Fig. 18 was similar to that obtained by Suzuki [11–13] for MEB occurring in copper mini/macrochannel that had many nucleation sites. It can be seen from this boiling curve that the microheater temperature was about 95 °C at ONB, which is also the crossing point of the boiling curves with highly smooth surface (square dots) and with eroded surface (circular dots). Visualization shows that MEB did not occur under this condition and nucleate boiling prevailed instead (see discussion below). However, with further increase in heat flux, MEB began to occur and these two boiling curves gradually merged. As shown in Fig. 18, when the heat flux was increased beyond 5 MW/m^2, there was not much difference between these two boiling curves when MEB occurred over the whole microheater on

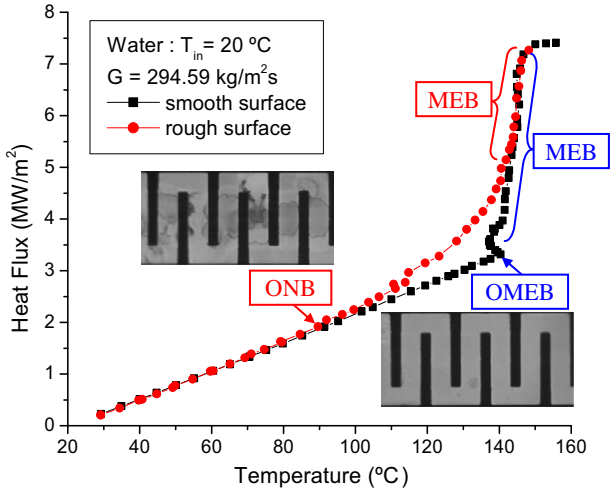

Fig. 18. Subcooled flow boiling curve of water in microchannels with smooth and rough surfaces at T_{in} = 20 °C and G = 294.6 kg/m^2 s.

both surfaces. This was because the microbubbles caused by bubble collapse served as bubble embryo, and therefore the heater surface condition did not have any effect on flow boiling.

Fig. 19a and b are a series of photos on the bubble behavior and the corresponding measurements of microheater temperature fluctuation during nucleate boiling on the eroded surface at q_{eff} = 2.77 MW/m^2, G = 294.6 kg/m^2 s and T_{in} = 20 °C. During the bubble growth of approximately 238 ms (Fig. 19a), it absorbed the latent heat of evaporation which caused decrease of 4 °C in heater temperature (Fig. 19b). As the bubble grew to approximately 140 μm in diameter, it detached from the heater and was flushed downstream (Fig. 19a) with increase in heater temperature (Fig. 19b). At a later time, another bubble occurred again, thus beginning a new cycle. A comparison between OMEB (Figs. 8 and 9) and ONB (Fig. 19) shows that (i) the occurrence of vapor bubble in OMEB and ONB caused decrease in microheater temperature; (ii) the vapor bubble size oscillated and collapsed into many fine bubbles in OMEB while the bubble grew to a certain size and was flushed downstream by incoming subcooled water in ONB.

3.4. Comparison between experimental data of MEB with existing heat transfer correlations

The experimental data shown in Fig. 13a will now be compared with two types of heat transfer correlations for subcooled flow boiling in macrochannels from the literature [23–29]. The first type of flow boiling correlations [23–26] gives an explicit relation between heat flux and temperature difference (usually in terms of wall superheat), in the form of $q = f(\Delta T)$, indicating that wall superheat was the dominant parameter in heat transfer other than mass flux or subcooling. The second type of flow boiling heat transfer correlations is the summation type correlation [27–29], which was first proposed by Chen [27] in the form of heat transfer coefficient $h = E \cdot h_1 + S \cdot h_2$ where the first term is the convective term with h_1 being the single-phase forced convection heat transfer correlation multiplied by an enhancement factor E. The second term is the evaporative term (a modification of the Forster and Zuber correlation [30] for pool boiling heat transfer h_2) multiplied by a suppression factor S.

Fig. 20a is a comparison of heat-flux data versus wall superheat data in the fully-developed MEB at three sets of mass flux G = 294.6, 589.2, 883.8 kg/m^2 s and T_{in} = 20 °C (taken from Fig. 13a) with first type of correlations by Jens and Lottes [23], Aladiev et al. [24], Thome et al. [25], and Labuntzov [26]. Fig. 20b is a plot of $\Delta T_{sat,pred}/\Delta T_{sat,expt}$ versus wall superheat, including information on its mean absolute error (MAE) which is defined as

$$\mathrm{MAE} = \frac{1}{M}\sum \frac{|\Delta T_{sat,pred} - \Delta T_{sat,expt}|}{\Delta T_{sat,expt}} \times 100\%,$$

where M is the number of data points. It can be seen that correlation given by Aladiev et al. [24] gives a closer agreement with a MAE of 9.8% while other correlations either underpredicted or overpredicted the wall superheat data with the MAE from 14% to 31.0%.

Fig. 21a shows the same set of data in terms of heat transfer coefficient in fully-developed MEB in comparison with the second type of boiling heat transfer coefficient correlations given by Chen [27], Gungor and Winterton [28], and Liu and Winterton [29]. Fig. 21b is a plot of h_{pred}/h_{expt} and the mean absolute error (MAE) versus wall superheat where

$$\mathrm{MAE} = \frac{1}{M}\sum \frac{|h_{expt} - h_{pred}|}{h_{exp}} \times 100\%$$

is also presented. It can be seen that all of these three existing correlations predicted the trend of the experimental heat transfer coef-

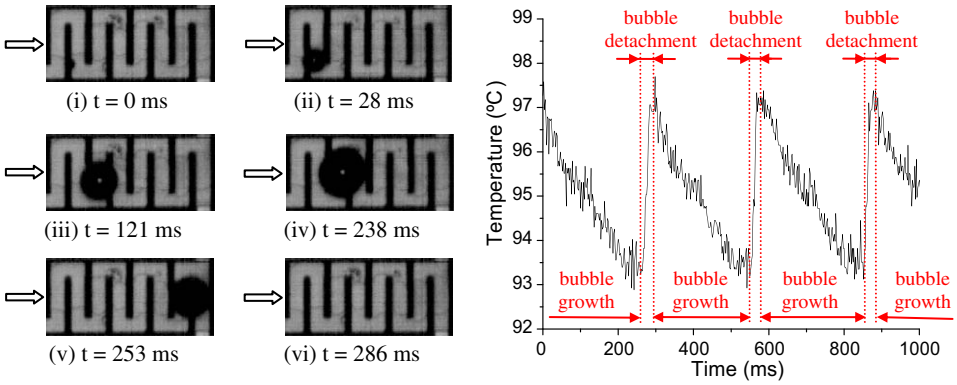

(a) Photos of bubble behavior in nucleate boiling taking at 5000 frame/s

(b) Measurement of the microheater temperature fluctuation

Fig. 19. Photos and temperature fluctuation in nucleate boiling in a microchannel with a rough heating surface at q_{eff} = 2.77 MW/m^2, G = 294.6 kg/m^2 s, and T_{in} = 20 °C.

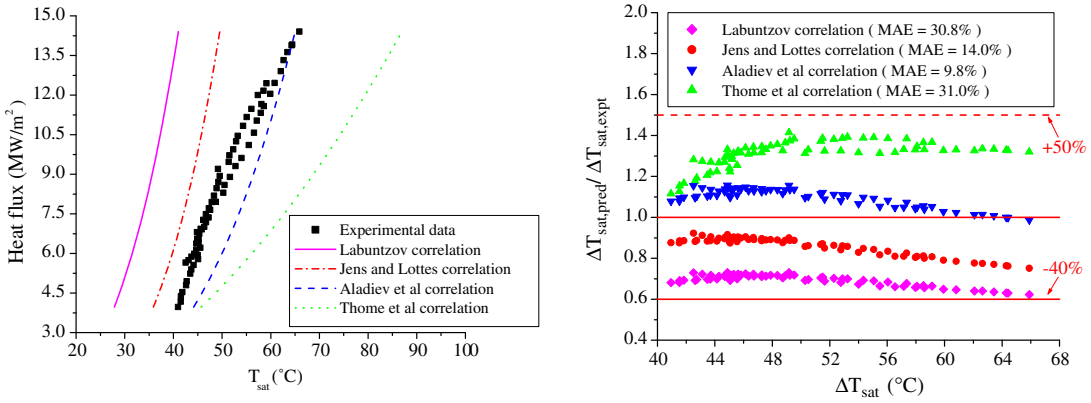

(a) Comparison of experiment data with existing correlations for flow boiling in macrochanels

(b) Wall superheat ratio versus wall superheat

Fig. 20. Comparison of subcooled flow boiling heat transfer data with preditions from correlations of Labuntzov [26], Jens and Lottes [23], Aladiev et al. [24], and Thome et al. [25].

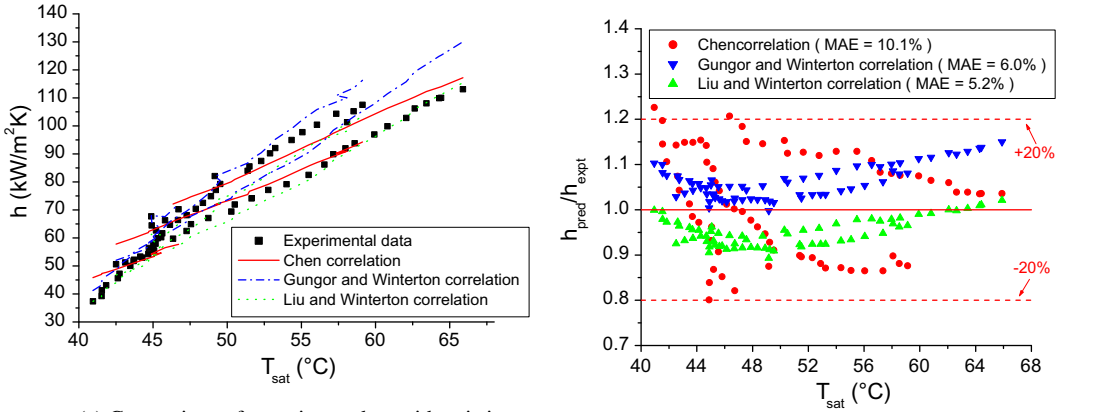

(a) Comparison of experiment data with existing correlations for flow boiling in mini/macrochanels

(b) Heat transfer coefficient ratio versus wall superheat

Fig. 21. Comparison of subcooled flow boiling heat transfer coefficient data with predictions from correlations of Chen [27], Gungor and Winterton [28] and Liu and Winterton [29].

ficient data in fully-developed MEB. Both the heat transfer correlations given by Gungor and Winterton [28] and Liu and Winterton [29] are in better agreement with the present data in MEB with the MAE of 6.0% and 5.2%, respectively, in comparison with Chen's correlation [27] with the MAE of 10.1%.

4. Concluding remarks

In this paper, microfabrication techniques were used to fabricate a microchannel integrated with a Pt microheater, which also served as a temperature sensor. Simultaneous visualization and measurements of temperature, heat flux and mass flux have been carried out to investigate subcooled flow boiling and microbubble emission boiling (MEB) phenomenon of water in a partially heated Pyrex glass wall in a microchannel having a hydraulic diameter of 155 μm with inlet temperature at 20, 60, and 80 °C, respectively.

The following conclusions can be drawn from the present work:

1. Visualization shows that a vapor bubble, on the wall of the microchannel, in contact with a highly subcooled liquid will break up into many micobubbles (from several micros to dozens of micros in diameter) due to condensation and instability of bubble interface between vapor and subcooled water. This microbubble emission boiling (MEB) phenomena occurred in a microchannel with a high inlet subcooling and at a high heat flux.
2. MEB is strongly affected by the degree of inlet water subcooling in the microchannel. At $G = 589.2\ \mathrm{kg/m^2\,s}$, although MEB occurred for $\Delta T_{sub} = 40$ and 60 °C, it did not occur for the case of $\Delta T_{sub} = 20$ °C. For this case of low inlet water subcooling where bubbles continue to grow and elongate without collapsing, and reversed flow was observed when the bubble touched the walls. The reversed flow of vapor led to periodical fluctuations of microheater temperature.
3. The occurrence of MEB in microchannel can remove a large amount of heat flux as high as 14.41 $\mathrm{MW/m^2}$ at $G = 883.8\ \mathrm{kg/m^2\,s}$ with only a moderate rise in wall temperature. Therefore, this heat transfer mode is very promising for next generation of chip cooling technology for microelectronic devices.
4. Developing MEB occurred when the initiation of MEB moved from downstream of the microheater to upstream of the microheater with a continuous decrease in wall temperature of the microheater at increasing heat flux. Fully-developed MEB occurred when the entire microheater was covered by MEB and a large increase in heat flux caused a small rise in the microheater temperature.
5. Although the mass flux and inlet water subcooling affected the magnitudes of heat flux versus temperature variations of the microheater in single-phase region significantly, the effects of mass flux and inlet water subcooling on the boiling curves in the fully-developed MEB regime are small.
6. After several runs of subcooled boiling experiments, it was found that occurrence of onset of MEB (OMEB) was considerably delayed due to the erosion of the surface resulting in many nucleate sites on the microheater surface. With further increase in heat flux after onset of nucleate boiling (ONB), OMEB began to occur. As the heat flux was increased further, fully-developed MEB occurred over entire microheater and the heater surface condition no longer has any effect on flow boiling.
7. Correlations by Gungor and Winterton [28] as well as by Liu and Winterton [29] for heat transfer in subcooled flow boiling in mini/macrochannels were found to be in better agreement with the fully-developed MEB in the present microchannel experiments with the MAE of 6.0% and 5.2% in comparison with Aladiev's correlation [24] and Chen's correlation [27] with the MAE of 9.8% and 10.1%, respectively.
8. The MEB phenomena on a Pyrex glass wall of a microchannel as observed in this experiment is somewhat different from those occurring in a copper mini/macrochannel as observed by Suzuki et al. [11–13], possibly due to different surface conditions. Also, Suzuki et al. [11–13] found that periodic MEB is usually accompanying with large inlet pressure oscillation with loud noise, which were not observed from this experiments. Thus, MEB in microchannel was more stable than those occurred in mini/macrochannels.

Acknowledgements

This work was supported by National Natural Science Foundation of China through Grant No. 50536010. The authors wish to thank Prof. K. Suzuki (Tokyo University of Science) for helpful discussion, and Mr. Hao Liang for his assistance in the numerical work.

References

[1] S. Nukiyama, Maximum and minimum values of heat transmitted from metal to boiling water under atmospheric pressure, Jpn. Soc. Mech. Eng. 37 (1934) 367–374.
[2] S.G. Kandlikar, Heat transfer characteristics in partial boiling, fully developed boiling, and significant void flow regions of subcooled flow boiling, J. Heat Transfer 120 (1998) 395–401.
[3] V. Prodanovic, D. Fraser, M. Salcudean, Bubble behavior in subcooled flow boiling of water at low pressures and low flow rates, Int. J. Multiphase Flow 28 (2002) 1–19.
[4] C.P. Yin, Y.Y. Yan, T.F. Lin, B.C. Yang, Subcooled flow boiling heat transfer of R-134a and bubble characteristics in a horizontal annular duct, Int. J. Heat Mass Transfer 43 (2000) 1885–1896.
[5] I.C. Bang, S.H. Chang, W.P. Baek, Visualization of the subcooled flow boiling of R-134a in a vertical rectangular channel with an electrically heated wall, Int. J. Heat Mass Transfer 47 (2004) 4349–4362.
[6] Y.M. Lie, T.F. Lin, Subcooled flow boiling heat transfer and associated bubble characteristics of R-134a in a narrow annular duct, Int. J. Heat Mass Transfer 49 (2006) 2077–2089.
[7] R.D. Boyd, Subcooled flow boiling critical heat flux (CHF) and its application to fusion energy components. Part I. A review of fundamental of CHF and related data base, Fusion Technol. 7 (1985) 7–31.
[8] S. Inada, Y. Miyasaka, S. Sakamoto, G.R. Chandratilleke, Liquid-solid contact state in subcooled pool transition boiling system, J. Heat Transfer 108 (1986) 219–221.
[9] M. Shoji, M. Yoshihara, Burnout heat flux of water on a thin wire, in: Proceedings of 28th National Heat Transfer Symposium of Japan, 1991, pp. 121–123.
[10] H. Wang, X.F. Peng, B.X. Wang, D.J. Lee, Jet flow phenomena during nucleate boiling, Int. J. Heat Mass Transfer 45 (2002) 1359–1363.
[11] K. Suzuki, R. Kawada, On subcooled flow boiling with microbubble emission in a horizontal circular channel, in The First International Symposium on Micro & Nano Technology, March 14–17, 2004, Honolulu, Hawaii, USA, 2004.
[12] K. Suzuki, Y. Gotoh, T. Kokubu, H. Kawamura, Microbubble emission boiling (characteristics of scale-up heating surface), in: The Sixth World Conference on Experimental Heat Transfer, Fluid Mechanics, and Thermodynamics, April 17–21, 2005, Matsushima, Miyagi, Japan, 2005.
[13] K. Suzuki, T. Kokubu, M. Nakano, H. Kawamura, I. Ueno, H. Shida, O. Ogawa, Enhancement of heat transfer in subcooled flow boiling with microbubble emission, Exp. Therm. Fluid Sci. 29 (2005) 827–832.
[14] M. Tange, S. Takagi, M. Watanabe, M. Shoji, Microbubble emission boiling in a microchannel and minichannel, Therm. Sci. Eng. 12 (2004) 23–29.
[15] H.Y. Wu, P. Cheng, Boiling instability in parallel silicon microchannels at different heat flux, Int. J. Heat Mass Transfer 47 (2004) 3631–3641.
[16] G. Hetsroni, A. Mosyak, E. Pogrebnyak, Z. Segal, Explosive boiling of water in parallel micro-channels, Int. J. Multiphase Flow 31 (2005) 371–392.
[17] G.D. Wang, P. Cheng, H.Y. Wu, Unstable and stable flow boiling in parallel microchannels and in a single microchannel, Int. J. Heat Mass Transfer 50 (2007) 4297–4310.
[18] J. Li, G.P. Peterson, P. Cheng, Three-dimensional analysis of heat transfer in a micro-heat sink with single phase flow, Int. J. Heat Mass Transfer 47 (2004) 4215–4231.
[19] T. Chen, J.N. Chung, An experimental study of miniature-scale pool boiling, J. Heat Transfer 125 (2003) 1074–1086.
[20] J. Li, P. Cheng, Bubble cavitation in a microchannel, Int. J. Heat Mass Transfer 47 (2004) 2689–2698.
[21] J. Li, G.P. Peterson, Boiling nucleation and two-phase flow patterns in forced liquid flow in microchannels, Int. J. Heat Mass Transfer 48 (2005) 4797–4810.
[22] R. Situ, Y. Mi, M. Ishii, M. Mori, Photographic study of bubble behaviors in forced convection subcooled boiling, Int. J. Heat Mass Transfer 47 (2004) 3659–3667.

[23] W.H. Jens, P.A. Lottes, An analysis of heat transfer, burnout, pressure drop and density data for high pressure water, Argonne Natl. Lab Report No. ANL-4627, 1951.
[24] I.T. Aladiev, L.D. Dodonov, U.S. Udalov, Teploenergetika 4 (9) (1957).
[25] J.R.S. Thom, W.M. Walker, T.A. Fallon, G.F.S. Reising, Boiling in subcooled water during flow up heated tubes or annuli, in: Proc. Inst. Mech. Eng., Manchester, UK, 1965.
[26] D.A. Labuntzov, Heat transfer problems with nucleate boiling of liquids, Therm. Eng. 9 (1972) 21–28.
[27] J.C. Chen, Correlation for boiling heat transfer to saturated fluids in convective flow, I & EC Process Des. Dev. 5 (1966) 322–329.
[28] K.E. Gungor, R.H.S. Winterton, A general correlation for flow boiling in tubes and annuli, Int. J. Heat Mass Transfer 29 (1986) 351–358.
[29] Z. Liu, R.H.S. Winterton, A general correlation for saturated and subcooled flow boiling in tubes and annuli, based on a nucleate pool boiling equation, Int. J. Heat Mass Transfer 34 (1991) 2759–2766.
[30] H.K. Forster, N. Zuber, Dynamics of vapour bubbles and boiling heat transfer, AIChE J. 1 (1955) 531–535.